5678 *Chem. Mater.* **2010,** *22,* 5678–5686
DOI:10.1021/cm1013653

CHEMISTRY OF MATERIALS
Article

Phosphine Oxide Based Electron Transporting and Hole Blocking Materials for Blue Electrophosphorescent Organic Light Emitting Devices

Amber L. Von Ruden, Lelia Cosimbescu, Evgueni Polikarpov, Phillip K. Koech, James S. Swensen, Liang Wang, Jens T. Darsell, and Asanga B. Padmaperuma*

Energy and Environment Directorate, Pacific Northwest National Laboratory, Richland, Washington 99352, United States

Received May 14, 2010. Revised Manuscript Received September 8, 2010

We report the design, synthesis, thermal, and photophysical properties of two phosphine oxide based electron transport/hole blocking materials, 2,6-bis(4-(diphenylphosphoryl)phenyl)pyridine (BM-A11) and 2,4-bis(4-(diphenyl-phosphoryl)phenyl)pyridine (BM-A10), for blue electrophosphorescent organic light emitting devices (OLEDs). The use of these materials in blue OLEDs with iridium(III) bis[(4,6-difluorophenyl)-pyridinato-$N,C^{2\prime}$]picolinate (Firpic) as the phosphor was demonstrated. Using the dual host device architecture with BM-A10 as the electron transport material (ETM) yields a maximum external quantum efficiency (EQE) of 8.9% with a power efficiency of 21.5 lm/W (4.0 V and 35 cd/m^2). When BM-A11 is used as the ETM, the maximum EQE and power efficiency improves to 14.9% and 48.4 lm/W, respectively (3.0 V and 40 cd/m^2).

Introduction

The development of efficient, stable organic solid-state white lighting has been an area of great interest in recent years as it has the potential to revolutionize current lighting systems and greatly reduce energy consumption.[1] A blue-emitting component is necessary for any method used in generating white light, whether it is down conversion or color mixing. However, due to efficiency and stability shortcomings, phosphorescent blue-emitting organic light emitting devices (OLEDs) still remain a challenge. State-of-the-art blue OLEDs comprise a phosphorescent dye doped into an ambipolar host material with a triplet energy higher than the phosphorescent dye. In such systems, internal quantum efficiency (QE) of up to 100% is reached by harvesting both singlet and triplet excitons.[2] For improved device efficiency in phosphorescent OLEDs, an ideal device needs to have a balanced number of carriers (electrons and holes) and the carriers need to be confined to the emissive region. As a result, blocking layers are used between host and charge transporting layers to confine electrons and holes as well as to prevent exciton leakage. The design and development of host and charge transporting materials is particularly challenging in the case of blue OLEDs in part because the triplet-state energy of these materials needs to be higher than that of the emitter to prevent exciton quenching.[3]

When designing electron transporting/hole blocking materials (HBMs), it is important that the materials have sufficiently deep highest occupied molecular orbital (HOMO) energies to block holes, in addition to triplet energies above the triplet energy of the emitter (> 2.7 eV in the case of FIrpic). Many HBMs that have deep enough HOMO energies to block holes are known but do not have favorable triplet excited state energies, making them inadequate for confining blue triplet excitons in the emissive layer (EML). We have already demonstrated that organic phosphine oxide (PO) materials exhibit excellent electron injection and hole and exciton blocking capabilities as well as good morphological stability.[4] In addition, PO materials can be designed to have high triplet energies and adjustable HOMO and lowest unoccupied molecular orbital (LUMO) energies for optimizing electron injection into and hole and exciton blocking for a variety of wide band gap host materials. Pyridine moieties have been shown to contribute to high electron transport ability[5] and, thus, were utilized in the molecular design of the reported HBMs. The electron deficient pyridine ring

*To whom correspondence should be addressed. Telephone: 509-372-4895. Fax: 509-375-2186. E-mail: asanga.padmaperuma@pnl.gov.

(1) Forrest, S. R. *IEEE J. Sel. Top. Quantum Electron.* **2000**, *6*, 1072.
(2) (a) Adachi, C.; Baldo, M.; Thompson, M. E.; Forrest, S. R. *J. Appl. Phys.* **2001**, *90*, 5048. (b) Kawamura, Y.; Goushi, K.; Brooks, J.; Brown, J. J.; Sasabe, H.; Adachi, C. *Appl. Phys. Lett.* **2005**, *86*, 071104.
(3) Adachi, C.; Kwong, R.; Djurovich, P.; Adamovich, V.; Baldo, M. A.; Thompson, M. E.; Forrest, S. R. *Appl. Phys. Lett.* **2001**, *79*, 2082.
(4) (a) Vecchi, P. A.; Padmaperuma, A. B.; Qiao, H.; Sapochak, L. S.; Burrows, P. E. *Org. Lett.* **2006**, *8*, 4211. (b) Padmaperuma, A. B.; Sapochak, L. S.; Burrows, P. E. *Chem. Mater.* **2006**, *18*, 2389. (c) Sapochak, L. S.; Padmaperuma, A. B.; Vecchi, P. A.; Qiao, H.; Burrows, P. E. *Proc. SPIE* **2006**, *6333*, 57. (d) Matsushima, T.; Adachi, C. *Appl. Phys. Lett.* **2006**, *89*, 253506. (e) Oyamada, T.; Sasabe, H.; Adachi, C.; Murase, S.; Tominaga, T.; Maeda, C. *Appl. Phys. Lett.* **2005**, *86*, 033053.
(5) (a) Tanaka, D.; Agata, Y.; Takeda, T.; Watanabe, S.; Kido, J. J. *J. Appl. Phys.* **2007**, *46*, L117. (b) Su, S.-J.; Sasabe, H.; Takeda, T.; Kido, J. *Chem. Mater.* **2008**, *20*, 1691. (c) Su, S.-J.; Chiba, T.; Takeda, T.; Kido, J. *Adv. Mater.* **2008**, *20*, 2125. (d) Sasabe, H.; Gonmori, E.; Chiba, T.; Li, Y.-J.; Tanaka, D.; Su, S.-J.; Takeda, T.; Pu, Y.-J.; Nakayama, K.; Kido, J. *Chem. Mater.* **2008**, *20*, 5951.

 Published on Web 09/29/2010

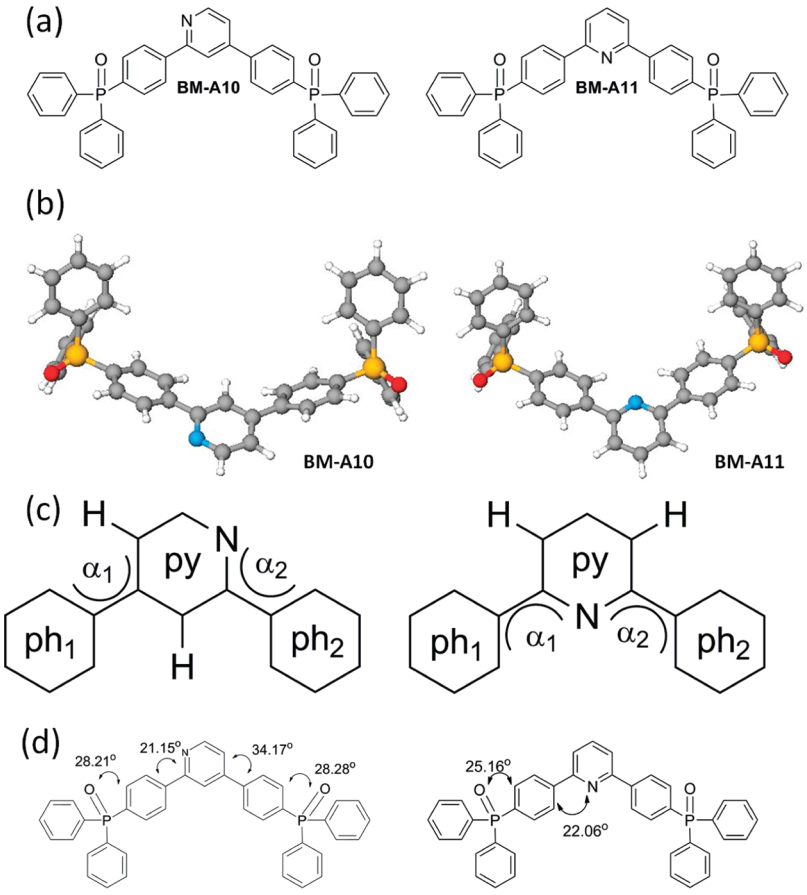

Figure 1. (a) Chemical structures and (b) optimized geometry of the blocking materials, by DFT calculations using the B3LYP model, with 6-31G* as the basis set. (c) Tortion angles between the phenyl and pyridyl rings of the blocking materials. (d) Structures of BM-A10 and BM-A11 with torsion angles.

lowers the LUMO energy which results in favorable electron injection from the cathode.

In this work, we report the synthesis of two new phosphine oxide based HBMs, 2,4-bis(4-(diphenyl-phosphoryl)-phenyl) pyridine (BM-A10) and 2,6-bis(4-(diphenylphosphoryl)phenyl)pyridine (BM-A11), with deep HOMO levels and triplet energies greater than 2.7 eV. The chemical structures and the optimized geometries of these two blocking materials are given in Figure 1. The materials are structural isomers, with BM-A11 containing a symmetrical pyridine diphenyl bridge while BM-A10 is asymmetrical with the phenyl groups attached at the 2,4 position relative to the pyridine which gives the blocking materials different electronic properties. Moreover, the difference in the shape of the molecule will most likely result in different packing in the solid state and film, hence a different charge transport in the device. A new class of phosphine-oxide based ambipolar host materials was developed and reported by our group that have good electron and hole transport properties that help maintain charge balance in the emissive zone.[6] The hole-blocking/electron-transporting materials BM-A10 and BM-A11 introduced in this paper were used in conjunction with the ambipolar host material 4-(diphenylphosphoryl)-*N*,*N*-diphenylaniline (HM-A1) and FIrpic as the emissive dopant.

(6) Polikarpov, E.; Swensen, J. S.; Chopra, N.; So, F.; Padmaperuma, A. B. *Appl. Phys. Lett.* **2009**, *94*, 223304.

Experimental Section

Synthesis and Characterization. All chemicals used in synthetic procedures were obtained from Aldrich Chemical Co. and used as received unless noted otherwise. Thermal analysis by differential scanning calorimetry (DSC) was obtained using a Netzsch simultaneous analyzer (STA 449 Jupiter). From these studies, both melting point and glass forming properties of BM-A11 and BM-A10 were determined. Sublimed samples (5 mg) were placed in aluminum pans and heated at 10 °C/min under N_2 gas at a flow rate of 50 mL/min. In, Sn, and CsCl was used as the temperature standard.

NMR spectra were obtained using a Varian Oxford 500 MHz spectrometer at the following frequencies: 499.8 MHz (^{1}H), 202.3 MHz (^{31}P), and 125.7 MHz (^{13}C). Tetramethylsilane was used as an internal reference for ^{1}H and ^{13}C spectra, and the ^{31}P signals were externally referenced to 85% H_3PO_4. Elemental analysis was performed by Columbia Analytical Services, Tuscon, AZ. Mass spectra (MS-ESI) were obtained using a Micromass Q-tof mass spectrometer.

The starting material 2,4-diiodopyridine for BM-A10 was prepared from commercially available 2,4-dichloropyridine according to published procedures,[7] while 2,6-dibromopyridine for BM-A11 was commercially available. The synthesis and characterization of the intermediate 2,6-bis(4-bromophenyl)pyridine is reported in published literature.[8] The intermediate for BM-A10,

(7) Schlosser, M.; Cottet, F. *Eur. J. Org. Chem.* **2002**, 4181.
(8) (a) Newkome, G. R.; Fishel, D. L. *J. Org. Chem.* **1972**, *37*, 1329. (b) Selbin, J.; Gutierrez, M. A. *J. Organomet. Chem.* **1983**, *246*, 95. (c) Kumar, A.; Rhodes, R. A.; Spychala, J.; Wilson, W. D.; Boykin, D. W.; Tidwell, R. R.; Dykstra, C. C.; Hall, J. E.; Jones, S. K.; Schinazi, R. F. Eur. J. Med. Chem. **1995**, *30*, 99. See Supporting Information for detailed synthesis.

2,4-bis(4-bromophenyl)pyridine,[9] was prepared via the standard Pd-catalyzed Suzuki-Miyaura coupling[10] reaction of 2,4-diiodopyridine and 4-bromophenylboronic acid.[11]

2,6-Bis(4-(diphenyl-phosphoryl)phenyl)pyridine (*BM-A11*). To a 3-neck round-bottom flask (RBF) was added 2,6-bis(4-bromophenyl)pyridine (2.50 g, 0.00643 mol, 1.0 equiv), and the flask flushed with argon. Anhydrous tetrahydrofuran (100 mL) was added, and the solution was cooled to −78 °C (dry ice: acetone bath). *N*-Butyllithium (6.4 mL, 0.0161 mol, 2.5 M in hexanes, 2.5 equiv) was added dropwise maintaining the temperature below −60 °C. The resulting dark solution was stirred cold for 4 h. Chlorodiphenylphosphine (2.6 mL, 0.0141 mol, 2.2 equiv) was added to give a pale yellow solution. The reaction mixture was allowed to warm to room temperature and stirred overnight. The reaction mixture was quenched with methanol, and solvents were removed to give a thick orange oil. The crude diphosphine was dissolved in 50 mL of methylene chloride in a flask affixed with a reflux condenser. To the stirred solution, 5 mL of 50% aqueous hydrogen peroxide was added slowly to prevent excessive foaming and bumping. The resulting mixture was stirred overnight at room temperature. The organic layer was washed with water and brine, and the extract was evaporated to dryness to afford a yellow thick residue which was purified by column chromatography (R_f = 0.10, SiO_2, hexanes/methanol/ethyl acetate = 6:1:2) to yield 1.60 g (35% over two steps) of chemically pure BM-A11. Mp: 279 °C (DSC, 10 K/min, N_2). ^{1}H NMR ($CDCl_3$, 295 K): δ 7.47−7.50 (m, 8H), 7.57 (t, 4H, J = 7.3 Hz), 7.69−7.73 (m, 8H), 7.77−7.83 (m, 6H), 7.89 (t, 1H, J = 7.8 Hz), 8.23 (dd, 4H, J = 2.5 Hz, 8.5 Hz). ^{13}C NMR ($CDCl_3$, 295 K): δ 120.1, 127.1 (J_{CP} = 12.3 Hz), 128.7 (J_{CP} = 11.6 Hz), 132.2 (J_{CP} = 10.1 Hz), 132.7 (J_{CP} = 10.1 Hz), 132.8, 133.0, 133.7, 138.1, 142.6, 156.0. ^{31}P NMR ($CDCl_3$, 295 K): δ 29.54. MS (ESI): M + H^+ Calcd. for $C_{41}H_{31}NO_2P_2$: 632.19 Found: 632.3872.

2,4-Bis(4-(diphenyl-phosphoryl)phenyl)pyridine (*BM-A10*). To a 3-neck RBF was added 2,4-bis(4-bromophenyl)pyridine (5.33 g, 0.0137 mol, 1.0 equiv), and the flask flushed with argon. Anhydrous tetrahydrofuran (125 mL) was added, and the solution was cooled to −78 °C (dry ice: acetone bath). *N*-Butyllithium (11.5 mL, 0.0288 mol, 2.5 M in hexanes, 2.1 equiv) was added dropwise maintaining the temperature below −60 °C. The resulting solution turned dark and was stirred cold for 4 h. Chlorodiphenylphosphine (5.3 mL, 0.0288 mol, 2.1 equiv) was added to give a pale yellow solution. The reaction mixture was allowed to warm to room temperature and was stirred overnight. The reaction mixture was quenched with methanol, and solvents were removed to give a thick orange oil. The crude diphosphine was dissolved in 100 mL of methylene chloride, and 10 mL of 50% aqueous hydrogen peroxide was added dropwise; the reaction mixture was stirred overnight at room temperature. The organic layer was washed with water and brine, and the extract was evaporated to dryness to afford a yellow residue which was purified by column chromatography (R_f = 0.12, SiO_2, hexanes/methanol/ethyl acetate = 6:1:2) to yield 3.67 g (42% over last two steps) of chemically pure BM-A10. Mp: 241 °C (DSC, 10 K/min, N_2). ^{1}H NMR ($CDCl_3$, 295 K): δ 7.47−7.51 (m, 8H), 7.55−7.60 (m, 4H), 7.69−7.73 (m, 8H), 7.77−7.85 (m, 7H), 7.96 (s, 1H), 8.14 (dd, 2H, J = 2.0 Hz, 8.5 Hz), 8.79 (d, 1H, J = 4.5 Hz). ^{13}C NMR ($CDCl_3$, 295 K): δ 119.4, 121.2, 127.2 (J_{CP} = 12.1 Hz), 127.4 (J_{CP} = 12.3 Hz), 128.7 (J_{CP} = 10.0 Hz), 128.8 (J_{CP} = 9.6 Hz), 131.9, 132.1, 132.2, 132.2, 132.3, 132.3, 132.3, 132.7, 132.8 (J_{CP} = 10.0 Hz), 132.9, 133.1 (J_{CP} = 10.0 Hz), 133.4, 133.8, 134.2, 141.8 (J_{CP} = 2.6 Hz), 142.7, 148.5, 150.7, 157.3. ^{31}P NMR ($CDCl_3$, 295 K): δ 29.14, 29.49. MS (ESI): M + H^+ Calcd. for $C_{41}H_{31}NO_2P_2$: 632.19 Found: 632.2740.

Computational Methods. All calculations were performed with the NWChem computational package[12] at the Environmental Molecular Sciences Laboratory. Ground-state geometries for the two blocking materials were fully optimized without any symmetry constrains by density-functional theory (DFT) calculations using the B3LYP model, with 6-31G* as the basis set. Molecular orbitals and bond lengths were visualized using Extensible Computational Chemistry Environment (ECCE),[13] a component of the Molecular Science Software Suite (MS^3) developed at Pacific Northwest National Laboratory.

Photophysical Characterization. UV−visible absorption spectra were collected on a Varian Cary 5 UV−vis−near infrared (NIR) spectrophotometer. Emission spectra were collected on a Horiba Jobin-Yvon Fluorolog Tau spectrofluorometer equipped with a Xenon lamp. Solution spectra were collected in 1 cm path length quartz cells for the concentration range 10^{-5}−10^{-3} M. Phosphorescence spectra were obtained in CH_2Cl_2 at 77 K at an excitation wavelength of 280 nm and time delay of 300 μs using a nanosecond optical parametric oscillator/amplifier operating at a 10 Hz repetition rate. The output was directed onto the sample, and emission was collected at right angles to the excitation and focused into a 1/8 m monochromator with a gated intensified CCD camera to record the spectra. The gate of the CCD camera could be set to reject scattered laser light and short-lived luminescence, allowing the observation of long-lived luminescence.

Electrochemical Characterization. Cyclic voltammetry was performed using a Princeton Applied Research EG&G potentiostat/galvanostat model 263 A, with a silver wire as the pseudoreference electrode, a Pt wire as the counter electrode, and glassy carbon as the working electrode. Reduction potentials were determined in anhydrous and degassed *N*,*N*-dimethylformamide (DMF) with 80 mM tetra(*n*-butyl)-ammonium hexafluorophosphate, 3 mM ferrocene, and 7 mM sample (scan speeds of

(9) ^{1}H NMR ($CDCl_3$, 295 K): δ 8.74 (d, 1H, J = 5.1 Hz), 7.94 (d, 2H, J = 8.5 Hz), 7.86 (s, 1H), 7.65 (m, 4H), 7.55 (d, 2H, J = 8.5 Hz), 7.43 (dd, 1H, J = 5.1 Hz, J = 1.6 Hz).

(10) Miyaura, N.; Suzuki, A. *Chem. Rev.* **1995**, *95*, 2457.
(11) Su, S.-J.; Chiba, T.; Takeda, T.; Kido, J. *Adv. Mater.* **2008**, *25*, 2125–2130.
(12) (a) Bylaska, E. J.; de Jong, W. A.; Govind, N.; Kowalski, K.; Straatsma, T. P.; Valiev, M.; Wang, D.; Apra, E.; Windus, T. L.; Hammond, J.; Nichols, P.; Hirata, S.; Hackler, M. T.; Zhao, Y.; Fan, P.-D.; Harrison, R. J.; Dupuis, M.; Smith, D. M. A.; Nieplocha, J.; Tipparaju, V.; Krishnan, M.; Wu, Q.; Van Voorhis, T.; Auer, A. A.; Nooijen, M.; Crosby, L. D.; Brown, E.; Cisneros, G.; Fann, G. I.; Fruchtl, H.; Garza, J.; Hirao, K.; Kendall, R.; Nichols, J. A.; Tsemekhman, K.; Wolinski, K.; Anchell, J.; Bernholdt, D.; Borowski, P.; Clark, T.; Clerc, D.; Dachsel, H.; Deegan, M.; Dyall, K.; Elwood, D.; Glendening, E.; Gutowski, M.; Hess, A.; Jaffe, J.; Johnson, B.; Ju, J.; Kobayashi, R.; Kutteh, R.; Lin, Z.; Littlefield, R.; Long, X.; Meng, B.; Nakajima, T.; Niu, S.; Pollack, L.; Rosing, M.; Sandrone, G.; Stave, M.; Taylor, H.; Thomas, G.; van Lenthe, J.; Wong, A.; Zhang, Z. *NWChem, A Computational Chemistry Package for Parallel Computer*, Version 5.1; Pacific Northwest National Laboratory: Richland, Washington, 2007. (b) Kendall, R. A.; Apr, E.; Bernholdt, D. E.; Bylaska, E. J.; Dupuis, M.; Fann, G. I.; Harrison, R. J.; Ju, J.; Nichols, J. A.; Nieplocha, J.; Straatsma, T. P.; Windus, T. L.; Wong, A. T. Comput. Phys. Commun., **2000**, *128*, 260−283.
(13) Black, G.; Daily, J.; Didier, B.; Elsethagen, T.; Feller, D.; Gracio, D.; Hackler, M.; Havre, S.; Jones, D.; Jurrus, E.; Keller, T.; Lansing, C.; Matsumoto, S.; Palmer, B.; Peterson, M.; Schuchardt, K.; Stephan, E.; Sun, L.; Swanson, K.; Taylor, H.; Thomas, G.; Vorpagel, E.; Windus, T.; Winters, C. *ECCE, A Problem Solving Environment for Computational Chemistry*, Software Version 4.5.1; Pacific Northwest National Laboratory: Richland, Washington, 2007.

Scheme 1. Synthetic Routes

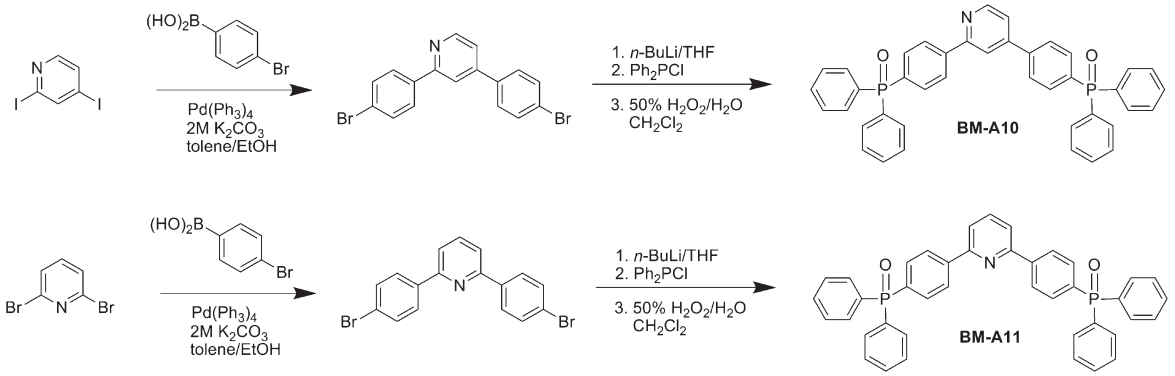

20−300 mV/s from −2.9 to +1.3 V). Reduction potentials were recorded relative to a ferrocenium/ferrocene (Fc^+/Fc) redox couple used as the internal reference.

OLED Characterization. Compounds HM-A1 (4-(diphenylphosphoryl)-*N*,*N*-diphenylaniline), BM-A11, and BM-A10 were purified by vacuum sublimation. TCTA (4,4′,4″-tris(carbazol-9-yl)-triphenylamine) was purchased from H.W. Sands (device grade) and used as received. TAPC (1,1-bis[(di-4-tolylamino)-phenyl]cyclohexane) was purchased from Kodak and vacuum-sublimed twice before use in the deposition system. OLEDs were fabricated on glass substrates precoated with a 100 nm thick layer of indium tin oxide having a sheet resistance of 15 Ohms/sq. The substrates were cleaned with detergent and water followed by organic solvents and, then, etched using oxygen plasma immediately prior to device fabrication. All organic and cathode layer depositions were performed by thermal evaporation in a high vacuum system (base pressure $< 3 \times 10^{-7}$ Torr). Film thicknesses were measured using a quartz crystal oscillator and calibrated using ellipsometry. Current−voltage characteristics were measured with an Agilent Technologies 4155B semiconductor parameter analyzer. Light output was measured using a Si photodetector placed behind the OLED. No corrections were made for light waveguided in the organic thin films or the substrate. Electroluminescence (EL) spectra were recorded with an Acton Research SpectrumM CCD mounted to an Acton Research monochromator.

Results and Discussion

Synthesis of blocking materials was accomplished using established procedures, first described by Baldwin.[14] A lithium−halogen exchange reaction between dibromoaryl bridge intermediates and *n*-butyllithium was followed by reaction with chlorodiphenylphosphine to give the crude diphosphines. The crude diphosphines were oxidized with H_2O_2 to give the diphosphine oxides BM-A10 and BM-A11 (Scheme 1). The crude products were first purified by column chromatography, and then, the chemically pure product was further purified by multiple high vacuum temperature gradient sublimations. During the first heating cycle, BM-A11 exhibited a single endothermic melting transition at 279 °C. After quenching the melted sample in liquid nitrogen, the second heating revealed a glass transition (Tg) at 102 °C. BM-A10, on the other hand, exhibited a glass transition at 109 °C followed by a crystallization exotherm (173 °C) and a single endothermic melting transition at 241 °C during the first heating. A second heating of this sample revealed only a glass transition (Tg) at 107 °C. Elemental analysis of BM-A10 reveals that there is a molecule of water present in BM-A10 even after high vacuum and temperature gradient sublimation.

(14) Baldwin, R. A.; Cheng, M. T. *J. Org. Chem.* **1967**, *32*, 1572.

Theoretical Analysis

Geometry. Ground-state geometries for the two blocking materials were fully optimized without any symmetry constrains by DFT calculations using the B3LYP model, with 6-31G* as the basis set. The optimized structures are shown in Figure 1b. Similar to previous reports of diphosphine oxide molecules, the polar P═O moieties showed an antiparallel arrangement with the oxygen atoms almost in plane with the central pyridine moiety. However, the P═O groups are orientated in a *cisoid* conformation with respect to the central aryl groups giving a computed net-dipole moment of 6.88 D and 3.10 D for BM-A10 and BM-A11, respectively. These two blocking materials are structural isomers of each other, but they have significantly different computed net-dipole moments, which is mostly determined by the direction of the two P═O moieties. BM-A11 is a somewhat symmetrical molecule where the P═O moiety is held at a torsion angle of 25.16° to the bridging phenyl ring. The two phenyl rings have a computed torsion angle of 22.06° (α_1,α_2) to the central pyridyl ring. Similarly, in BM-A10, the P═O moieties are held at a torsion angle of 28.21° and 28.28° to the respective bridging phenyl ring. The significant difference in the conformation of these molecules is at the central pyridyl rings, as shown in Figure 1c. The torsion angles between the phenyl rings and the pyridyl for BM-A10 are 34.17° (α_1) and 21.15° (α_2). The orientation of the ph_2 ring with respect to BM-A10 is similar to that of BM-A11 due to the fact that the phenyl ring is attached at the ortho position relative to N in pyridine. If this was a C−H group, then the sterics of the two hydrogen atoms would cause the torsion angle to increase, as evident by the α_1 in BM-A10. This change in the torsion angles of the aryl rings of the two molecules could very well influence the π-orbital overlap and the electron transport.

Electronic Properties. The computed band energy and orbital amplitude plots for the two HOMOs and the two

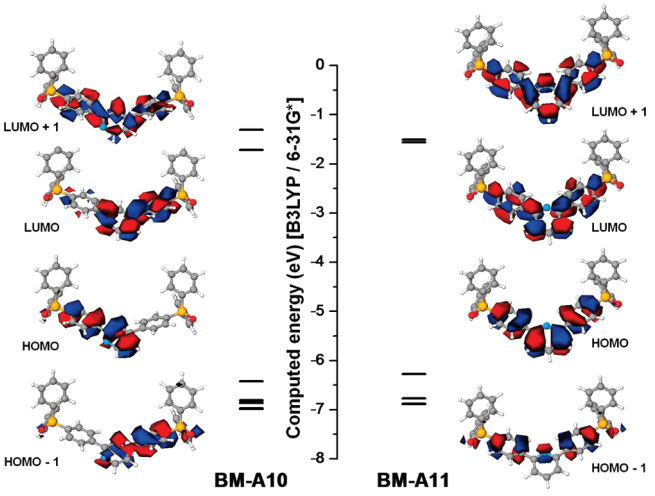

Figure 2. Computed energy levels and the orbital amplitude plots for the blocking materials.

LUMOs of the blocking materials are depicted in Figure 2. The electron density is localized predominately on the bridging diphenyl pyridine (ph_2py) system for the symmetrical BM-A11. This is similar to what was observed for other PO based blocking materials.[15] Because the P═O moiety acts as a point of saturation and prevents electronic communication between the ph_2py bridge and outer phenyl groups, the photophysics of BM-A11 are expected to be representative of the ph_2py chromophore. The asymmetric nature of the ph_2py bridge on BM-A10 is evident in the electronic delocalization as well. Both the HOMO and the LUMO density of states of the molecule are delocalized over the pyridyl ring and one phenyl ring.

Electrochemistry and Photophysical Results

To experimentally confirm the trends in predicted orbital energies, it is necessary to carry out cyclic voltametry (CV). The experimental electrochemical reduction potential is converted to the LUMO energy relative to vacuum, using a reference compound as described by Kolosov.[16] For our purposes, 4,4-(*N*,*N*-dicarbazoyl)biphenyl (CBP) was used for the reference with $E_{1/2}^{red}$ (CBP) = −2.77 V and E_{LUMO} = −2.7 eV according to Kolosov's published work. Since substitution of organic chromophores with inductively electron withdrawing P═O moieties lowers both the HOMO and LUMO energies of the bridging chromophore, electrochemical oxidation has been difficult to obtain in most common solvents. As a result, only the reduction potentials are listed in Table 1. The electrochemically estimated E_{LUMO} and the onset of optical absorption (E_g) measured in solution were used to estimate the E_{HOMO} state. Both blocking materials have HOMO energies deep enough to be useful as hole blocking materials. BM-A10 has a deeper LUMO than that of BM-A11 which is in accordance with the theoretically predicted values.

Table 1. Reduction Potentials from Cyclic Voltammetry (CV), Estimated HOMO and LUMO Energies, Theoretically Predicted HOMO and LUMO Energies, and Experimentally Measured Optical Band Gap (E_g) and Triplet Exciton Energies (E_T)

	from cyclic voltammetry			theoretical values			
				B3LYP/6-31G*		B3LYP/cc-pVDZ	
	$E_{1/2}^{red}$ (V)[a]	E_{LUMO} (eV)[b]	E_{HOMO} (eV)[c]	E_{LUMO} (eV)	E_{HOMO} (eV)	E_{LUMO} (eV)	E_{HOMO} (eV)
BM-A10	−2.26	−3.2	−7.0	−1.7	−6.4	−1.9	−6.6
BM-A11	−2.36	−3.1	−6.8	−1.6	−6.2	−1.7	−6.4

	experimental (eV)		theoretical values				
			$S_1 \leftarrow S_0$ (eV)		$T_1 \leftarrow S_0$ (eV)		E_g (eV)[f]
	E_g[d]	E_T[e]	6-31G*	cc-pVDZ	6-31G*	cc-pVDZ	cc-pVDZ
BM-A10	3.8	2.8	4.21	4.16	3.02	2.99	4.7
BM-A11	3.7	2.7	4.16	4.10	2.95	2.91	4.7

[a] First half-electron reduction potential in DMF using Fc^+/Fc internal reference. [b] Calculated using the following equation: $E_{LUMO} = -e[E_{1/2}^{red}\text{ (CBP)} - E_{1/2}^{red}\text{ (sample)} + 2.7]$ eV. [c] Calculated using the following equation: $E_{HOMO} = E_{LUMO} + E_g$. [d] E_g estimated from the absorption edge of the experimental absorbance spectrum. [e] $\nu_{0,0}$ peak from the emission spectrum recorded at 77K. [f] $E_g = |E_{HOMO} - E_{LUMO}|$.

The photophysical data collected for dichloromethane solutions at room temperature are shown in Figure 3. Fluorescence at room temperature is weak for both BM-A10 and BM-A11, with λ_{max} ~345−350 nm. The emission profiles of both materials are similar, whereas the lowest energy absorbance bands are not. In order to explain the experimental absorbance spectra, time dependent density functional theory (TD-DFT, B3LYP/6-31G*) studies were carried out. For BM-A10, the lowest energy transition is a $S_1 \leftarrow S_0$ centered at 4.21 eV (oscillator strength, f = 0.27). The strongest transition is the $S_2 \leftarrow S_0$ centered at 4.60 eV (f = 0.73). Thus, the lowest energy transition is only seen as a shoulder for BM-A10. For BM-A11, the strongest transition is also the lowest energy transition which is attributed to a $S_1 \leftarrow S_0$ transition centered at 4.16 eV (f = 0.46). This transition is followed by a $S_2 \leftarrow S_0$ transition centered at 4.44 eV (f = 0.27). As a result, the lowest energy region of BM-A11 spectrum exhibits more resolved transitions than BM-A10. Computations carried out at a more advanced basis set (cc-pVDZ) do not change the trends predicted at 6-31G*. Solution absorption and emission spectra of BM-A10 and BM-A11 were measured in several solvents with varying polarities. No change in absorption or emission spectra of the PO HBMs as a function of solvent polarity is observed, which suggests the dipole moments do not change significantly upon electronic excitation. The lack of solvent dependence is consistent with previous observations for other di-PO materials. The absorbance spectra of the bridging diphenyl pyridyl units are also plotted with the di-PO compounds. Each of the fragments has similar bands as the di-PO compounds, but the latter is lower in energy, as seen for other di-PO compounds.[17]

(15) Sapochak, L. S.; Padmaperuma, A. B.; Vecchi, P. A.; Cai, X.; Burrows, P. E. *Proc. SPIE* **2007**, *6655*, 65506.
(16) Kolosov, D.; Adamovich, V.; Djurovich, P. I.; Thompson, M. E.; Adachi, C. *J. Am. Chem. Soc.* **2002**, *124*, 9945.
(17) Padmaperuma, A. B.; Sapochak, L. S.; Burrows, P. E. *Chem. Mater.* **2006**, *18*, 2389.

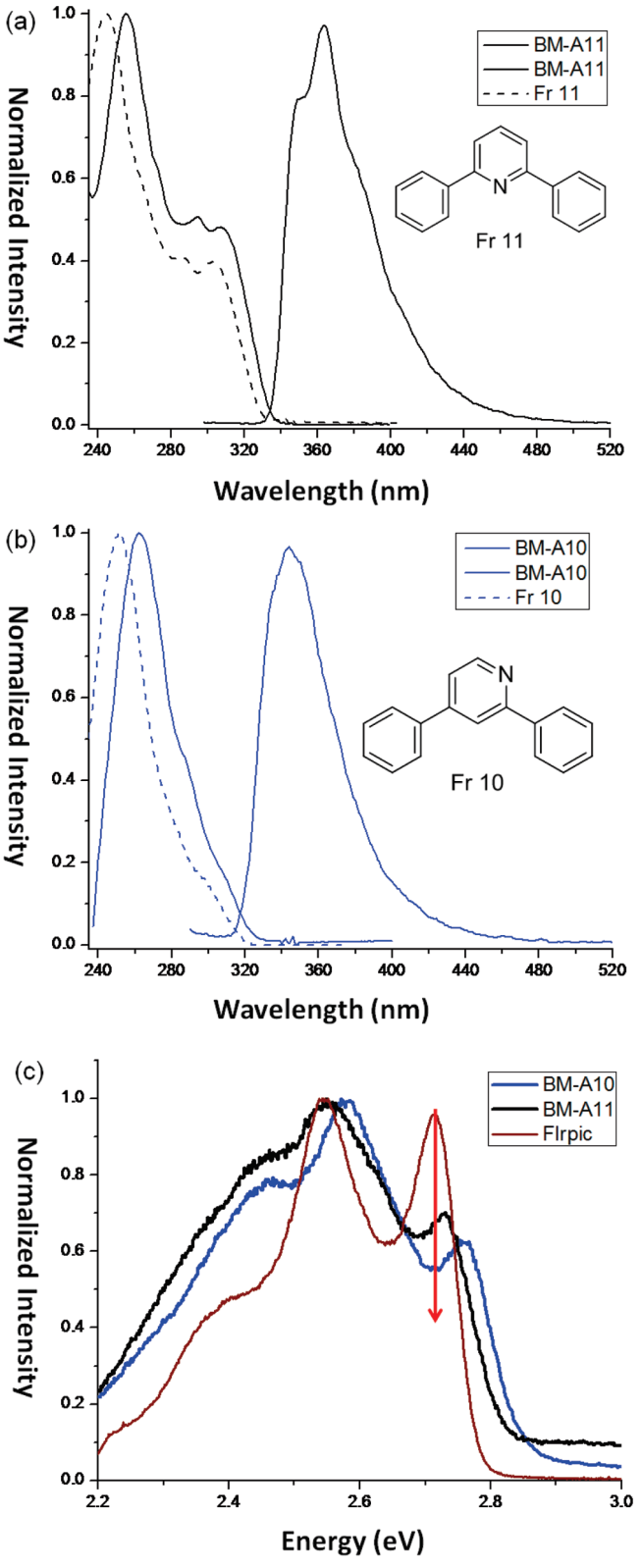

Figure 3. Room temperature absorption and emission of (a) BM-A10 and (b) BM-A11 compared to their bridging fragments in 10^{-5} M CH_2Cl_2 solution. (c) Low temperature phosphorescence spectra for BM-A10, BM-A11, and FIrpic.

For these materials to be used as blocking materials for blue OLEDs, they need to have a triplet energy higher than that of FIrpic (2.71 eV). Low temperature delayed emission studies were carried out to estimate the triplet energies for BMs. The method described by Turro was used to extract the triplet energy value.[18] The low temperature phosphorescence spectra as well as the emission spectrum of FIrpic are given in Figure 3c. The triplet energies for both BM-A10 and BM-A11 were found to be greater than that of FIrpic which ensures that the HBMs will not quench FIrpic excitons. The energy of the $T_1 \leftarrow S_0$ transition for both BM-A10 and BM-A11 was calculated at the B3LYP level using 6-31G* and cc-pVDZ as the basis sets. (Table 1) Although the predicted values were not identical to the measured values, they followed the same trend.

Blue OLED Studies

Single Carrier Studies. In order to compare the electron transport for BM-A10 and BM-A11, single carrier (electron only) devices were fabricated and evaluated. These devices had the following architecture: indium tin oxide (ITO)/20 nm Al/x nm BM/1 nm LiF/100 nm Al where BM is either BM-A10 or BM-A11 and x = 130 or 160. The thin layer of Al placed between the ITO and the BM materials eliminated hole injection from the ITO into the BM materials and ensured that these were electron only devices. Here, we investigate the charge transport behavior of electron only devices at different thicknesses in order to reveal any possible effect by injection barrier at organic-metal contact. In Figure 4a, the current density vs electric field data of either BM-A10 or BM-A11 exhibit consistency for different thicknesses, indicating that injection barrier (if existing) does not play a significant role in the charge transport of the single carrier device. Therefore, single carrier devices demonstrated in Figure 4a are operated under bulk-limited condition rather than injection-limited condition. As seen from Figure 4a, BM-A11 shows superior current density as the function of electric field, compared to BM-A10. It is, thus, conclusive that BM-A11 possesses higher bulk conductivity than BM-A10. Since both BMA11 and BMA10 layers are undoped so that charge carrier density is low in both materials, we can derive that the electron transport mobility in BM-A11 is higher than that in BM-A10. Further work to extract mobility value from charge transport data of single carrier device is ongoing in this group and will be published elsewhere.

Single Host Device Studies. The usefulness of BM-A10 and BM-A11 as blocking materials was studied in simple heterostructure OLEDs. An ambipolar host molecule HM-A1[6] was used as the host for the phosphorescent emitter FIrpic, and either BM-A10 or BM-A11 was used as the hole blocking/electron transporting material in the OLED stack [device structure, ITO/30 nm TAPC/5 nm TCTA/15 nm 5 wt % FIrpic−HM-A1/50 nm BM/1 nm LiF/100 nm Al where BM is either BM-A10 or BM-A11]. The layer thicknesses of the HTL and the ETL were optimized for FIrpic−HM-A1 system as reported previously.[6] The emission for these devices was exclusively

(18) Turro, N. J. *Modern Molecular Photochemistry*; University Science Books, 1991; ISBN: 0935702717.

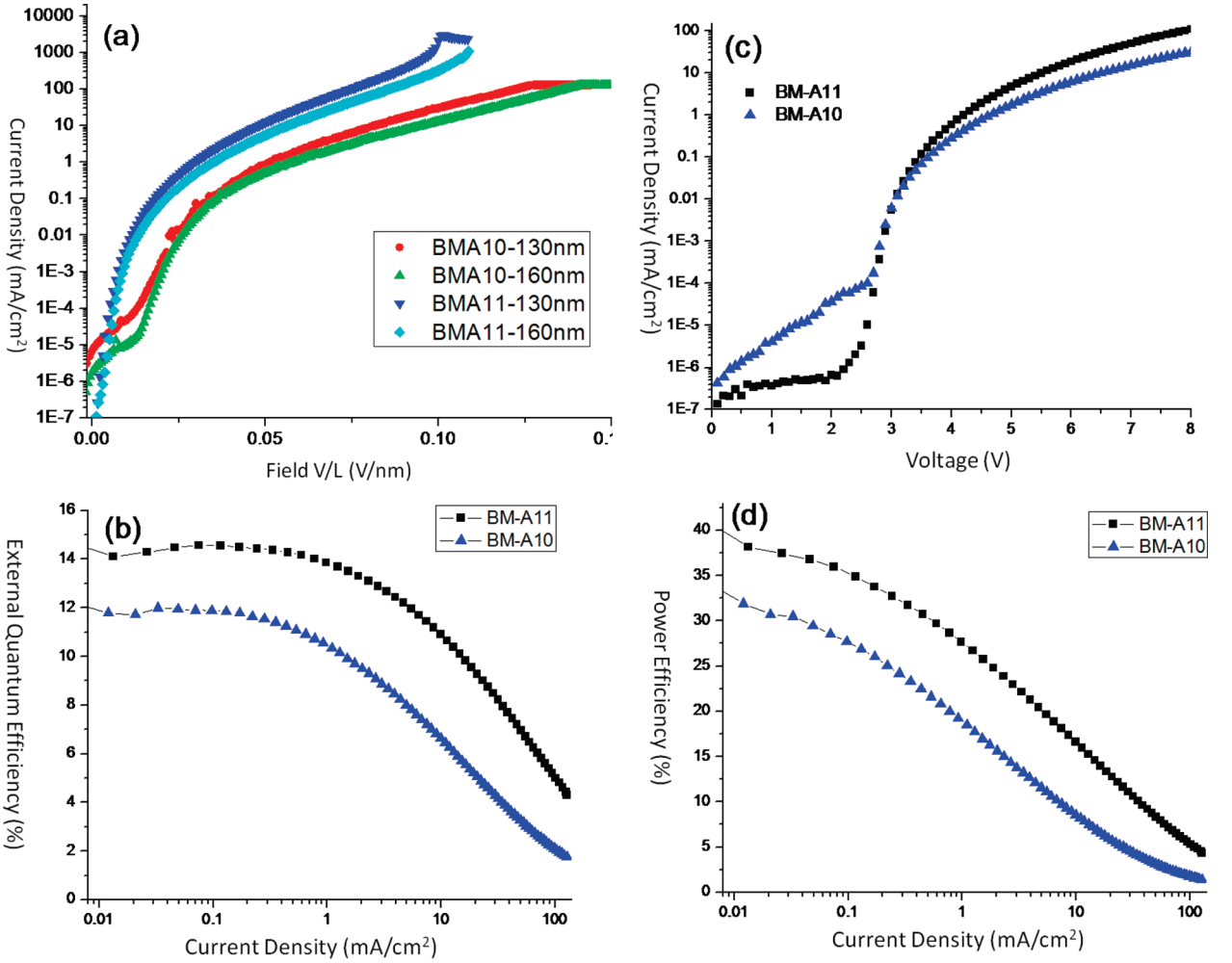

Figure 4. (a) Electron only data (current density vs electric field) for the single carrier BM-A10 and BM-A11 devices: ITO/20 nm Al/x nm BM/1 nm LiF/100 nm Al, x = 130 or 160. (b) EQE vs current density, (c) current density vs voltage, and (d) power efficiency vs current density, for blue phosphorescent OLEDs fabricated using BM-A10 (squares) and BM-A11 (triangles) as the hole blocking-electron transporting layer: ITO/30 nm TAPC/5 nm TCTA/15 nm HM-A1:5% FIrpic/50 nm BM/1 nm LiF/100 nm Al where BM is either BM-A10 or BM-A11.

from FIrpic, suggesting the ability of the BMs to transport electrons as well as to block holes. The current density as a function of voltage (panel c) and the external quantum efficiency as a function of current density (panel b) are shown in Figure 4. Table 2 highlights device performance at 1 mA/cm^2. OLEDs using BM-A11 have lower drive voltages and higher brightness and efficiency than OLEDs using BM-A10.

The only difference in the OLEDs for the data shown in Figure 4b−d is the use of different hole blocking/electron transporting layers with same thicknesses. The disparity in the current density vs voltage characteristics (Figure 4c) is, therefore, due to the difference in electron transport by the two blocking materials. It is worth noting that charge transport is closely related to the charge mobility of the materials, and thus, ultimately to packing and morphology of the molecule. We found interesting structural properties of these isomers, and further studies are needed to correlate their structure differences with their behavior in a device. Since BM-A11 has better electron transport, more electrons make it through the ETL and into the emissive layer, resulting in a greater overall current density during device operation.

The greater external quantum efficiency (EQE) and power efficiency for the OLEDs fabricated using BM-A11 rather than for those using BM-A10 (Figure 4b,d) is also a result of the better electron transport in BM-A11. The hole transport material TAPC used in these devices is known to have high hole mobility.[19] In the OLEDs where BM-A11 is used as the blocking layer, more electron density reaches the emissive layer than when BM-A10 is used as the HBL due to BM-A11's better electron transport, resulting in better charge balance in the emissive region. Hence, brightness and, thus, the efficiencies of the BM-A11 devices are higher than the BM-A10 devices.

As discussed previously, both BM-A10 and BM-A11 provide good hole blocking properties because of their deep HOMO levels. It is known that the emission zone for OLEDs using HM-A1, the host used in this work, is near the interface between the emissive layer and the hole blocking-election transporting layer because HM-A1 preferentially transports holes.[20] With the emission zone

(19) Aonuma, M.; Oyamada, T.; Sasabe, H.; Miki, T.; Adachi, C. *Apply. Phys. Lett.* **2007**, *90*, 183503.
(20) Polikarpov, E.; Swensen, J. S.; Cosimbescu, L.; Koech, P. K.; Rainbolt, J. E.; Padmaperuma, A. B. *Appl. Phys. Lett.* **2010**, *96*, 053306.

Table 2. Device Properties[a]

	voltage (V)	EQE (%)	power efficiency (lm/W)	brightness (cd/m^2)
BM-A10	4.63 ± 0.02	10.2 ± 0.4	18.4 ± 0.7	270
BM-A11	4.21 ± 0.01	13.7 ± 0.3	27.3 ± 0.6	365

[a] Data reported at a current density of 1 mA/cm^2; 30 nm TAPC/5 nm TCTA/15 nm HMA1:5%FIrpic/50 nm BM/1 nm LiF/100 nm Al.

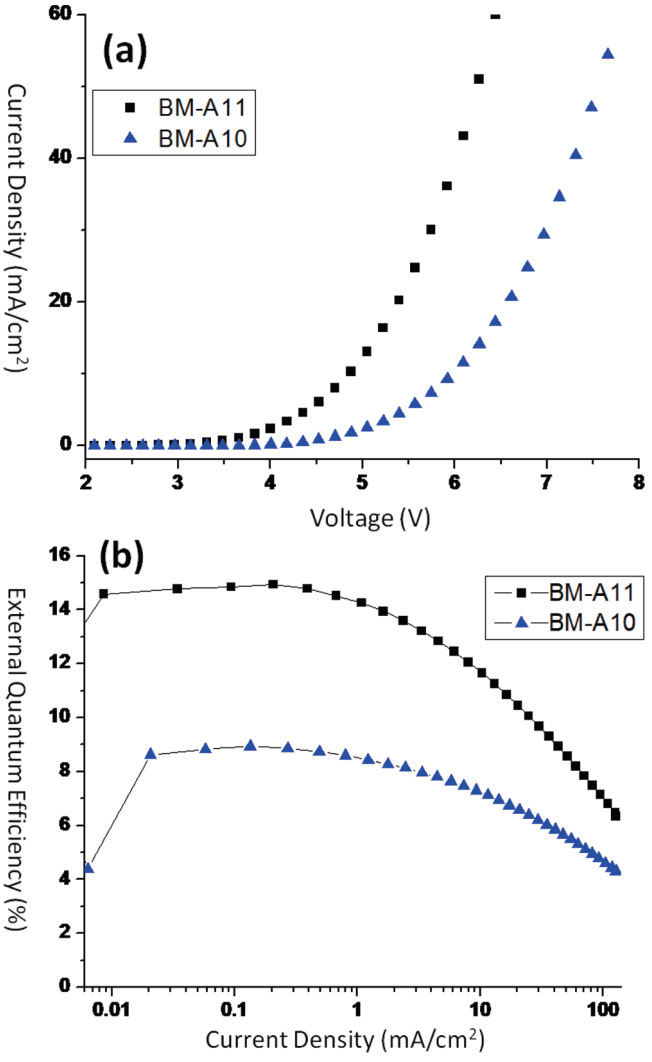

Figure 5. (a) Current density vs voltage and (b) EQE vs current density for blue phosphorescent dual host OLEDs fabricated using BM-A10 and BM-A11 as the transporting material. Device structure: ITO/35 nm TAPC/15 nm 5 wt % FIrpic:60% BM:35% TAPC/50 nm BM/1 nm LiF/100 nm Al.

so close to the hole blocking/electron transporting layer, the hole blocking properties are very important. Without good hole blocking, significant hole leakage into the electron transporting layer would occur, resulting in decreased OLED brightness and efficiency.[21]

Dual Host OLED Studies. Dual hosts systems were demonstrated previously by blending of HTM and electron transport material (ETM) with the intent to eliminate interfaces and injection barriers and, thus, improve device efficiency. The dual host emissive layer can improve charge balance by varying the ratio of the two coevaporated host materials.[22] This is particularly beneficial for phosphorescent OLEDs, as it has been demonstrated that efficiency roll-off depends strongly on charge balance for iridium dopant based phosphorescent devices.[23] In this study, we used the BMs as the ETL to form a dual host layer with TAPC and FIrpic as the emitter. The device structure studied for these materials was ITO/35 nm TAPC/15 nm 5 wt % FIrpic:60% BM:35% TAPC/50 nm BM/1 nm LiF/100 nm Al. The emission from these devices was exclusively from FIrpic, indicating the ability of the BM to block the triplet exciton of FIrpic. Even in this device configuration, BM-A11 outperformed BM-A10 in both EQE and voltage (Figure 5). The dual host devices with BM-A10 as the ETM have a maximum EQE of 8.9% with a power efficiency of 21.5 lm/W (4.0 V and 35 cd/m^2). At a current density of 1 mA/cm^2 (4.6 V and 265 cd/m^2), the EQE is 8.6%, with a corresponding power efficiency of 18.1 lm/W. When BM-A11 is used as the ETM, the maximum EQE and power efficiency improves to 14.9% and 48.4 lm/W, respectively (3.0 V and 40 cd/m^2). At a current density of 1 mA/cm^2, these devices exhibit an EQE and power efficiency of 14.2% and 37.8 lm/W, respectively, at a voltage of 3.6 V. (J = 1 mA/cm^2, 435 cd/m^2).

Conclusions

The synthesis and characterization of two new phosphine oxide electron transport/hole blocking materials are reported. The BMs have sufficiently deep HOMO energies to block holes and high enough triplet energies to prevent exciton quenching. These materials have the chemical functionality to transport electrons and were used as the electron transport/hole blocking layer in blue electro phosphorescent OLED devices. Although the two materials have similar structures and similar electronic properties, the device properties vary. The attachment of the phenyl rings to the central pyridyl ring is different in the two molecules, and this difference causes the two molecules to pack differently which could very well influence the π-orbital overlap and lead to differences in electron transporting ability and overall device properties.

Acknowledgment. This work was funded by the Solid Sate Lighting Program of the U.S. Dept. of Energy, within the Building Technologies Program (BT), Award No. M68004043, and managed by the National Energy Technology Laboratory (NETL). We thank Dr. A. Joly for the assistance in collecting low temperature phosphorescence spectra. We would also like to thank Dr. S. Burton and Dr. R. Zhang for assistance in NMR and mass spectroscopy. A portion of this research was performed using the Environmental Molecular Sciences Laboratory (EMSL), which is a national scientific user facility sponsored by the Department of Energy's Office of Biological and Environmental Research and is located at Pacific Northwest National

(21) Kido, J.; Ohtaki, C.; Hongawa, K.; Okuyama, K.; Nagai, K. *Jpn. J. Appl. Phys.* **1993**, *32*, L917.
(22) Lin, T.-C.; Hsiao, C.-H.; Lee, J.-H. Proc. of SPIE *5937*, 59371Q-1.
(23) Giebink, N. C.; Forrest, S. R. *Phys. Rev. B* **2008**, *77*, 235215.

Laboratory (PNNL). Computations were carried out using "NWChem, A Computational Chemistry Package for Parallel Computers, Version 5.1″ (2007), developed at the High Performance Computational Chemistry Group, Pacific Northwest National Laboratory, Richland, Washington 99352-0999, USA. Extensible Computational Chemistry Environment (ECCE), A Problem Solving Environment for Computational Chemistry, Software Version 6.0″ (2009), as developed and distributed by Pacific Northwest National Laboratory, P.O. Box 999, Richland, Washington 99352, USA, and funded by the U.S. Department of Energy, was used to obtain some of these results. Pacific Northwest National Laboratory (PNNL) is operated by Battelle Memorial Institute for the U.S. Department of Energy (DOE) under Contract No. DE-AC06-76RLO 1830.

Supporting Information Available: NMR spectra; DSC versus temperature figure; table of CV data; current versus potential figures (PDF). This material is available free of charge via the Internet at http://pubs.acs.org.